Caliphate Journal of Science & Technology (CaJoST)

ISSN: 2705-313X (**PRINT**); 2705-3121 (**ONLINE**) **Research Article**

Open Access Journal available at: https://cajost.com.ng/index.php/files and https://www.ajol.info/index.php/cajost/index

This work is licensed under a Creative Commons Attribution-NonCommercial 4.0 International License.

DOI: https://dx.doi.org/10.4314/cajost.v6i3.5

Article Info

Received: 25th June 2024

Revised: 28th October 2024

Accepted: 7th November 2024

Photon attenuation properties of samarium-doped zinc bismuth silicate glass: A study using Cs-137, Co-60, and Na-22 Radiation Sources

Usman Iliyasu[1], Mukhtar Bature[2], Muttaka Umar[1], Usman Abubakar[1], Anas Shehu[1]

[1]Department of Physics, Sokoto State University, Sokoto Nigeria
[2]Department of Physics, Federal University Gusau, Nigeria

***Corresponding author's email:**

usman.iliyasu@ssu.edu.ng

Cite this: *CaJoST*, 2024, 3, 281-288

The photon attenuation properties of the samarium-doped zinc bismuth silicate (ZBSS) glass series were investigated, revealing a strong composition-dependent behavior. The ZBSS10 sample, with the highest Bi_2O_3 content, demonstrated the highest linear attenuation coefficient (LAC) of 2.829 cm^{-1} at 0.284 MeV. However, the LAC decreases with increasing photon energy, as higher-energy photons penetrate deeper into the glass. The Mean Free Path (MFP) increases as Bi_2O_3 content decreases, allowing photons to travel farther before interaction with atoms. At 0.284 MeV, ZBSS10 (0.931 wt% Bi_2O_3) had the shortest MFP of 0.353 cm, while ZBSS50 (0.741 wt% of Bi_2O_3) had MFP of 0.455 cm, representing a 28.9% increase. The elastic moduli enhanced with increasing SiO_2 levels, and Poisson's ratio showed a significant increase with rising SiO_2 content, indicating an improved mechanical property. The sample ZBSS50, with the highest SiO_2 level, shows an enhanced fast neutron effective removal cross-section, surpassing other samples in the series. Both ZBSS10 and ZBSS50 provide excellent photon and neutron shielding, making them superior to some standard shielding materials and ideal for radiation protection applications.

Keywords: Cesium-137; Cobalt-60; Sodium-22; Silicate glass; Phy-X/PSD; Mean free path.

1. Introduction

Photon attenuation, the reduction in intensity of ionizing radiation as it interacts with matter, is a fundamental process with significant implications for various fields, including. Traditional shielding materials like lead glasses have been widely used due to their high attenuation efficiency, but their toxicity and environmental concerns have limited their applications [1-4]. The development of alternative materials with tailored photon attenuation properties is crucial for safer and more sustainable radiation shielding and detection solutions. Samarium-doped zinc bismuth silicate glass, a novel material with potential applications in radiation detection and shielding, has shown promising properties.

SiO_2 (silicon dioxide) is a network former, forming a rigid three-dimensional structure of Si-O-Si bonds., capable of forming covalent bonds with heavy metal and transition metal oxides to produce glasses that exhibit exceptional transparency in the visible light spectrum, making them ideal for various optical applications [3]. SiO_2 exhibits high viscosity and can form glass without crystallizing, making it an ideal material for glass production. Its exceptional resistance to thermal expansion and high softening point make it the most widely available and easiest glass to manufacture commercially [5]. While SiO_2 requires high temperatures to reach its glass transition temperature, the addition of ZnO can alter the network structure, weakening the connections and thereby lowering the glass transition temperature T_g and increasing the optical transparency [6, 7]. The Zn^{2+} occupy potential nucleation sites, making it harder for crystallization.

The incorporation of Bi_2O_3 into the glass network leads to the formation of Bi-O bonds, which introduces excess oxygen ions and increases the average bond length. resulting in creation of non-bridging oxygen (NBO) sites [8]. While the coordination environments (BiO_6 and BiO_3) of bismuth ions (Bi^{3+}) participating in silicate glass formation, enable the creation of specialized glasses with tailored properties for applications like optics, electronics, and biomedical materials [9]. According to Abou et al. [10], the addition of Bi_2O_3 into glass structure significantly enhances its photon radiation shielding capabilities and improve the attenuation properties due to bismuth high atomic number (Z=83) and density (8.9 g/cm³), which increases the probability of interactions while enhancing radiation absorption and scattering.

 © 2024 Faculty of Science, Sokoto State University, Sokoto.

Sm^{3+} ions are in the +3-oxidation state, which is typical for rare earth ions like samarium. Sm^{3+} ions are usually surrounded by six or eight oxygen ions, forming an octahedral (six-fold) or cubic (eight-fold) coordination, respectively [11]. adding Sm^{3+} ions into the glass structure act as network modifiers, breaking up the Si-O-Si bonds and forming Sm-O-Si bonds, which alters the glass structure and properties. Glass designed for photon shielding must be formulated to possess high mechanical strength and thermal resistance, enabling it to withstand the harsh conditions associated with radiation exposure. Moreover, careful selection of glass composition is crucial, as different formulations exhibit varying radiation absorption properties, which impact the amount of heat generated during irradiation. By optimizing glass composition and properties, the glass can effectively absorb radiation while maintaining its structural integrity and optical properties, ensuring reliable performance in photon shielding applications. Sm^{3+} ions have been found to decrease thermal conductivity, reducing heat transfer and improving thermal insulation due to the large atomic mass, which reduces the velocity of phonons (quantized sound waves) in the glass, leading to decreased thermal conductivity. Furthermore, it can create localized vibrations in the glass network, scattering phonons, while reducing thermal conductivity.

This study investigates the photon attenuation properties of samarium doped zinc-bismuth-silicate glass using three standard energy sources: Cs(137), Co(60), and Na(22). By examining the attenuation coefficients and related parameters, this research aims to contribute to the understanding of the material's radiation interactions and its potential as a lead-free shielding material, addressing the growing demand for safer and environmentally friendly radiation protection solutions. To accomplish this, we employ the Phy-X/PSD software to compute the radiation protection parameters utilizing the standard radiation sources including Cs-137 (cesium-137), Co-60 (cobalt-60), and Na-22 (sodium-22). These sources emit radiation at specific energies, allowing us to determine the relevant protection parameters. The Phy-X/PSD is an adequate substitute for experimental techniques and is one of the most efficient approaches. Abouhaswa et al. [12] utilized the Phy-X software to calculate shielding parameters of WO_3 doped borate glasses. Similarly, Alburiahi et al. [13] calculate the shielding parameters of lead sodium borate glass using Phy-X and Geant4 software. Deviation in the MAC values were less than 1%, indicating the accuracy of Phy-X software.

2. Materials and Methods

2.1 Glass synthesis and physical properties

The glasses were prepared using the conventional melt-and-quench techniques, as described by Pal et al. [14]. The compositions were formulated as $xSiO_2$+20ZnO+0.5Sm_2O_3+(79.5-x)Bi_2O_3, where x varied from 10 to 50 mol%. The melt was achieved at 1150°C for 40 minutes using an electric furnace. Subsequently, the molten glass was rapidly quenched using high-purity stainless-steel molds at room temperature to alleviate stress and fatigue. Further details on density, molar volume, emission spectra, absorption spectra, and Judd–Ofelt intensity are reported elsewhere [14]. Table 1 is a description of weight fraction of the compounds, elemental composition, and densities.

Table 1. Material composition of the ZBSS glass

Glass code	Weight fraction compound (wt%)				Element weight fraction (wt%)					Density
	ZnO	Bi_2O_3	SiO_2	Sm_2O_3	Zn	O	Bi	Si	Sm	g/cm^3
ZBSS10	0.047	0.931	0.017	0.005	0.038	0.038	0.038	0.038	0.038	6.89
ZBSS20	0.053	0.902	0.039	0.006	0.043	0.125	0.809	0.018	0.005	6.64
ZBSS30	0.060	0.867	0.066	0.006	0.048	0.137	0.778	0.031	0.006	6.54
ZBSS40	0.072	0.072	0.072	0.072	0.058	0.156	0.730	0.050	0.007	6.46
ZBSS50	0.088	0.741	0.162	0.009	0.070	0.181	0.665	0.076	0.008	6.28

2.2 Elastic and mechanical properties

The elastic properties of the investigated glasses were done using the Makishima-Mackenzie's model [15]. The model relates the molar volume (V_m), density (ρ), dissociation energy (G_i), and atomic packing factor (V_i) of the glass. The total dissociation energy of the glass mixture can be calculated from the following equation [16]:

$$G_T = \sum_i G_i w_i \quad (1)$$

where $\sum_i G_i w_i$ represent sum of the total dissociation energy and molar weight fraction w_i of

 © 2024 Faculty of Science, Sokoto State University, Sokoto.

the ith component over all the glass mixture components.

Young Modulus is related to the total packing density and total dissociation energy via the expression [16]:

$$E = 8.36 V_T G_T \quad (2)$$

where V_T represent the total atomic packing density and can be expressed as:

$$V_T = \frac{\rho}{M} \sum_i w_i V_i \quad (3)$$

where V_i represent the packing factor and can be calculated from the following relation for the metal oxide of the form $A_X O_Y$

$$V_i = N_A \frac{4}{3\pi} (X {R_A}^3 + Y {R_O}^3) \quad (4)$$

where R_A and R_O is the ionic radii for the metal and oxygen. The bulk modulus K_T ,shear modulus S_T , and longitudinal L_T can be expressed from the following relations [17]:

$$K_T = 10\, V_T^2 G_T \quad (5)$$

$$S_T = \frac{3K_T}{10.2V_T - 1} \quad (6)$$

$$L_T = K_T + \frac{4S_T}{3} \quad (7)$$

The Poisson's ration P_r, hardness H_m, and fractional bond connectivity can be expressed from the following equations [16]:

$$P_r = 0.5 - \frac{1}{7V_T} \quad (8)$$

$$H = \frac{(1-2P_r)E_T}{6(1+P)} \quad (9)$$

$$F_b = 4\frac{S_T}{K_T} \quad (10)$$

2.3 Phy-X/PSD software

Photon Shielding and Dosimetry (PSD) software well known as Phy-X/PSD is ~~a~~ user-friendly for simulation of shielding parameters available at https://phy-x.net/PSD [18]. The Phy-X/PSD user interface presents a dialog checkbox where an individual is prompt to enter the chemical composition and density of each sample after initial registration. The software provides an energy range of up to 1GeV and an interface for selecting shielding parameters of interest.

Saleh et al. [19] utilized XCOM software to calculate the nuclear radiation shielding properties of lithium lead bismuth borate glass and compare with Phy-X/PSD software. The shielding parameters show a good agreement with less than 1% deviation. Also, Al-Buriahi utilized Phy-X/PSD to investigate the shielding performance of lead sodium borate glass and compare with Geant4 simulation results. The results show a good agreement and the total percentage deviation was reported to be less than a unity. The linear attenuation coefficient (LAC, μ) is a fundamental parameter that describes the probability of absorption of monoenergetic photons per unit thickness of a material. It is defined as the fraction of incident photons that are absorbed or scattered per unit distance travelled in the material, and is expressed as [20, 21].

$$I = I_o e^{\mu t} \quad (11)$$

where I represent the fraction of photons after interaction with an absorber, I_o represent the incident photon intensity before interaction with an absorber material, μ is a constant called the linear attenuation coefficient (cm^{-1}) of the absorbing material and t is the material thickness (cm).

Half value layer HVL, represents the amount of material necessary to attenuate the photon beam to 50% of its initial intensity [22, 23].

$$HVL = {Ln2}/{\mu} \quad (12)$$

The Mean Free Path (MFP) is a parameter that describes the average distance travelled by photons in an absorber material before undergoing a successful interaction, such as absorption or scattering. It represents the average path length that a photon travels in the material before interacting with an atom or molecule [20].

$$MFP = {1}/{\mu} \quad (13)$$

Radiation protection efficiency RPE, is a measure of how well a material or structure reduces the intensity of ionizing radiation. The radiation protection efficiency of any defensive glass can be calculated by following equation [24]:

$$RPE = \left(1 - \frac{I_o}{I}\right) \times 100 \quad (14)$$

3. Results and Discussion

The study investigates the physical, mechanical, and radiation shielding properties of $xSiO_2$+20ZnO+0.5Sm_2O_3+(79.5-x)Bi_2O_3 glass system, assessing its potential for ionizing radiation shielding applications. The mechanical properties indicate that increasing Si_2O notably enhances the glass's physical and mechanical properties, as evidenced by improved Youngs, shear, bulk, and Poison ration, as shown in Table 2.

 © 2024 Faculty of Science, Sokoto State University, Sokoto.

Table 2. Elastic and mechanical properties of ZBSS glass

Glass sample code	V_T (cm^3/mol)	G_I (KJ/mol)	E_T (Gpa)	K_T (Gpa)	S_T (Gpa)	L_T (Gpa)	P_r	H(Gpa)	F
ZBSS10	0.409	86.40	295.43	144.53	455.68	752.11	0.151	29.89	12.61
ZBSS20	0.495	88.542	366.40	216.95	535.81	931.37	0.211	29.10	9.88
ZBSS30	0.634	86.422	458.06	347.38	635.43	1194.62	0.275	26.99	7.32
ZBSS40	0.884	86.202	637.05	673.63	840.27	1794.00	0.338	25.64	4.99
ZBSS50	0.891	88.482	659.08	702.44	868.48	1860.41	0.340	26.29	4.95

From Table *2*, the mechanical properties of the glasses improve as SiO_2 content increases and Bi_2O_3 content decreases. This enhancement is attributed to a reduction in defects and improved glass stability, leading to better elastic properties and a more robust glass structure [25]. As the

SiO_2 content increases, the energy required to break the bond rises from 86.40 to 88.482 kJ/mol, indicating enhanced thermal and mechanical stability. The elastic moduli (E_T, K_T, S_T, and L_T as shown in Table *2*) also increase linearly, further improving the mechanical properties of the glass. Additionally, the fractional bond length decreases from 12.61 to 4.95 kJ/mol, signifying increased stiffness and hardness, which enables the material to better resist stress and degradation. The increase in mechanical properties can be attributed to Higher Bond Strength of Si-O, which are stronger than Bi-O bonds. As the proportion of SiO_2 increases, the overall bond strength in the glass increases, contributing to greater thermal and mechanical stability. The increase in Poisson ratio from 0.151 (ZBSS10) to 0.340 (ZBSS50) as SiO_2 increases can be attributed to the increase in the interconnected network, forming a stable network, which allows for greater lateral expansion when subjected to uniaxial stress, resulting in a higher Poisson's ratio. The micro-hardness (H) decreases from 29.89 (ZBSS10) to 26.29 (ZBSS50) due to a more rigid structure that is less capable of resisting localized stress concentrations. This complex interplay between the network structure, bonding characteristics, and overall composition influences the mechanical behavior of the glass.

The linear attenuation coefficient (LAC) of ZBSS10 is 2.829 cm^{-1}, which is greater than the values of 2.666 cm^{-1} for ZBSS20, 2.553 cm^{-1} for ZBSS30, 2.413 cm^{-1} for ZBSS40, and 2.20 cm^{-1} for ZBSS50, due to the highest Bi_2O_3 level in ZBSS10. The high weight fraction of Bi_2O_3 (0.931 wt%) in ZBSS10 means that there are more Bi_2O_3 molecules per unit volume, providing more opportunities for photon interactions. This increases the probability of interactions between photons and the glass, resulting in higher LAC value. At lower photon energies, for instance, at 0.284 MeV, the interaction mechanism is governed by photoelectric effects enabling higher photon absorption, because the energy of the incoming photons is closer to the binding energies of electrons in the glass material. normally, high atomic element like bismuth, typically have lower binding energies for their electrons, enhancing the photoelectric effect at lower energies and leading to higher absorption coefficients for photons as observed in sample ZBSS10. While at higher photon energies, Compton scattering (0.662-1.173 MeV) and above 1.275 MeV pair production dominates the interaction process leading to reduced absorption coefficient, attributed to decreasing probability of photon interactions.

Table 3. Linear attenuation coefficient of the BZSS glass as a function of photon energy.

		Glass code				
Photon source	Energy (MeV)	ZBSS10	ZBSS20	ZBSS30	ZBSS40	ZBSS50
Cs (137)	0.284	2.829	2.666	2.553	2.413	2.200
Co (60)	0.347	1.907	1.802	1.733	1.648	1.516
Na (22)	0.511	1.020	0.970	0.941	0.906	0.851
Cs (137)	0.662	0.735	0.702	0.684	0.665	0.631
Co (60)	0.826	0.581	0.556	0.544	0.532	0.510
Co (60)	1.173	0.426	0.410	0.402	0.396	0.383
Na (22)	1.275	0.400	0.385	0.379	0.373	0.362
Co (60)	1.333	0.389	0.374	0.368	0.363	0.351
Co (60)	2.506	0.297	0.286	0.281	0.276	0.267

 © 2024 Faculty of Science, Sokoto State University, Sokoto.

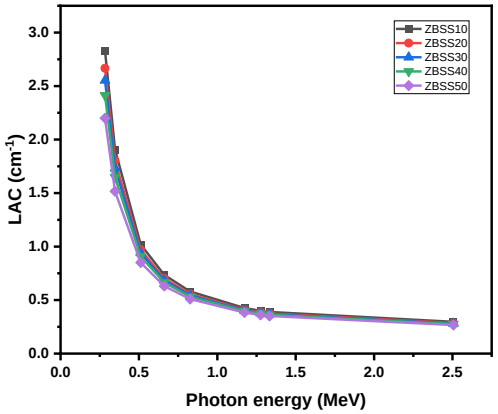

Figure 1. LAC of ZBSS glass as a function of photon energy.

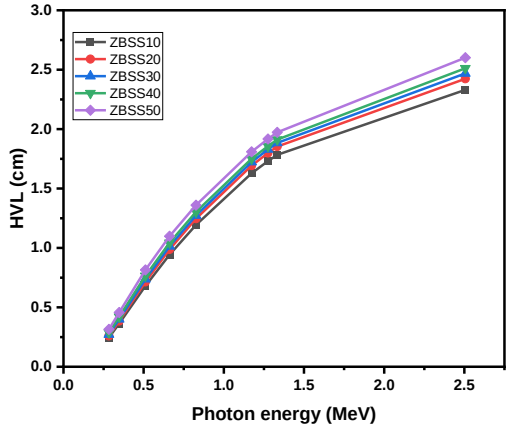

Figure 2. HVL as function of photon energy.

The Half-Value Layer (HVL) is an important parameter in radiation shielding optimization, because it represents the thickness of the material required to reduce the intensity of radiation by half. A smaller HVL of a material, indicates better radiation attenuation capabilities. As shown in Figure 2, ZBSS10, which has the highest bismuth concentration, exhibits the lowest HVL value. This can be attributed to the higher density of ZBSS10 (6.89 g/cm^3),

indicating that more atoms are packed together per unit volume. This increased atomic density enhances the interaction with incident photons, leading to a higher probability of photon absorption, Consequently, reducing HVL. Although the ZBSS10 sample has a higher molar volume (48.45 cm^3/mol), it surprisingly exhibits the lowest HVL among the samples. This seemingly contradictory behavior can be attributed to the sample's exceptionally high density. Despite the larger molar volume, the density of ZBSS10 is high enough to compensate for the increased volume, resulting in a higher probability of photon interactions and ultimately leading to a lower HVL. In other words, the denser packing of atoms in ZBSS10 outweighs the effect of its larger molar volume, making it the most effective at attenuating radiation This anomaly can be attributed to the larger atomic size of bismuth ions (Bi^{3+}) compared to silicon ions (Si^{4+}), leading to a greater molar volume, moreover, Bi_2O_3 has the highest of 0.931 wt% in the ZBSS10 structure compared to SiO_2. Furthermore, the coordination number of Bi^{3+} may differ from that of Si^{4+}, influencing the packing efficiency and resulting in a larger molar volume. These factors contribute to the observed increase in molar volume for ZBSS10. At 0.284 MeV, ZBSS10 has lowest HVL of 0.245 cm, while ZBSS20, ZBSS30, ZBSS40, and ZBSS50 are 0.260, 0.271, 0.287, and 0.315 cm, respectively as depicted in Figure 2. As a result, ZBSS10 requires 22.2% less thickness than ZBSS50 to achieve the same level of radiation attenuation, making it a more efficient radiation shielding material while lowering material cost, and decreased weight and increased portability.

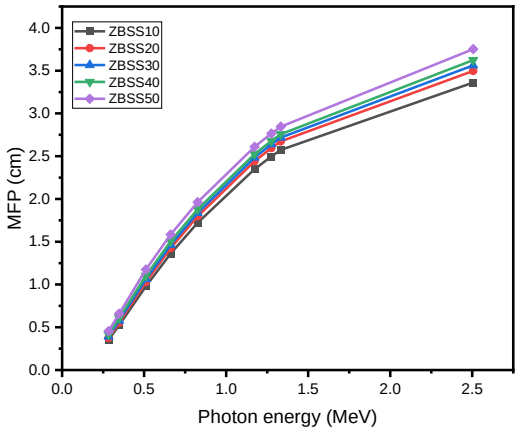

Figure 3. mean free part as a function of photon energy

We investigated the mean free path for all the five samples, The mean free path (MFP) of photons in a material plays a significant role in determining its attenuation properties. In the investigated glass with decreasing Bi_2O_3 content: the MFP of photons increases, allowing them to travel farther within the material before interacting with an atom. At a photon energy of 0.284 MeV, ZBSS10, with the highest Bi_2O_3 content (0.931 wt%), exhibited the shortest mean free path (MFP) of 0.353 cm, whereas ZBSS50, with the lowest Bi_2O_3 content (0.741 wt%), had an MFP of 0.455 cm, representing an increase of approximately 28.9 % in ZBSS50 as the Bi_2O_3 content decreased from 0.931 wt% to 0.741 wt%. Similarly, at 2.506 MeV, the MFP is larger for ZBSS50. This finding is consistent with the Half-Value Layer (HVL) results, which demonstrate the significant impact of Bi_2O_3 on photon attenuation. Our result also aligns with the previous report by Almuqrin et al, [26], further

 © 2024 Faculty of Science, Sokoto State University, Sokoto.

validating the role of Bi_2O_3 in enhancing radiation shielding capabilities.

Radiation protection efficiency (RPE) is essential for ensuring optimal radiation protection, safety, and efficiency across various applications. Using the values of the HVL of the investigated glass, at photon energy of 0.284 MeV, the following thicknesses are required to achieve specific reductions in incident photon intensity: 25% reduction: 0.021 cm (ZBSS10) and 0.030 cm (ZBSS50), 50% reduction: 0.051 cm (ZBSS10) and 0.072 cm (ZBSS50), 75% reduction: 0.103 cm (ZBSS10) and 0.145 cm (ZBSS50), and 90% reduction: 0.174 cm (ZBSS10) and 0.246 cm (ZBSS50), respectively. while at 2.506 MeV, 25% reduction: 0.205 cm (ZBSS10) and 0.251 cm (ZBSS50), 50% reduction: 0.488 (ZBSS10) and 0.597 cm (ZBSS50), 75% reduction: 0.978 cm (ZBSS10) and 1.193 cm (ZBSS50), and 90% reduction: 1.662 cm (ZBSS10) and 2.028 cm (ZBSS50), respectively as shown in Figure 4. The degree of photon attenuation in a specific glass is directly related to its composition and thickness, and photon energy, as shown in Figure 4. This results, demonstrates that material thickness and composition play a significant role in determining the extent of photon absorption.

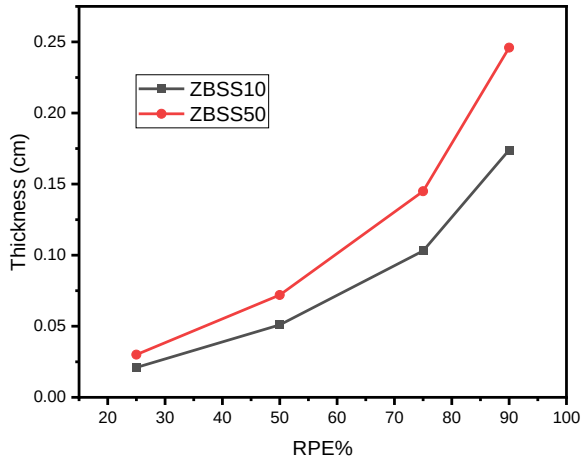

Figure 4. Radiation protection efficiency as a function of glass thickness.

These results emphasize the crucial role of the HVL in determining the optimal material thickness needed for effective radiation protection efficiency (RPE). HVL measurements offer valuable insights into the material's radiation-absorbing capabilities, facilitating the selection of appropriate thicknesses for efficient radiation shielding and protection

The fast neutron effective removal cross-section ($\sum_R$) in glass is essential for shielding, as it reflects the glass's capacity to absorb and eliminate fast neutrons. High-energy neutrons can penetrate deeply into materials and cause damage. The effective fast neutron removal cross-section was calculated using the equation proposed by Abd et al. [27]:

$$\sum_R(cm^2/g) = 0.190Z^{-0.743} \ (Z \leq 8) \quad (15)$$

$$\sum_R(cm^2/g) = 0.125Z^{-0.565} \ (Z > 8) \quad (16)$$

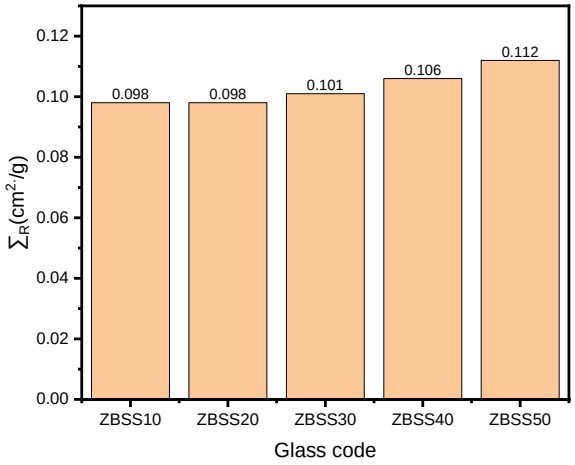

Figure 5. effective fast neutron removal cross sections of ZBSS glass.

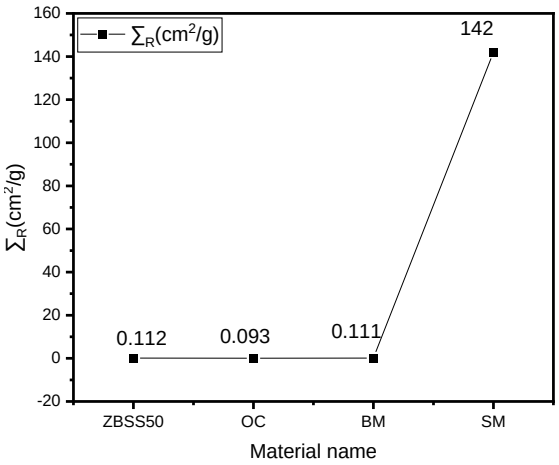

Figure 6. Comparison of effective fast neutron removal cross sections of ZBSS50 with ordinary concrete (OC), Basalt magnetite (BM), and steel magnetite (SM).

Figure 5 shows that the fast neutron removal cross-sections increase with higher SiO_2 content, because SiO_2 has a higher neutron absorption cross-section than Bi_2O_3, enhancing its effectiveness in neutron absorption. The elevated SiO_2 content in ZBSS50 may result in a denser and more rigid glass structure, as shown in Table *2*, which promotes more effective neutron scattering and absorption.

 © 2024 Faculty of Science, Sokoto State University, Sokoto.

Consequently, ZBSS50, with its higher SiO_2 and lower Bi_2O_3 content, exhibits the highest fast neutron effective removal cross-section among the ZBSS series, making it a highly effective material for fast neutron absorption. Figure 6 demonstrates a comparison of ZBSS50 with standard neutron-absorbing materials. Ordinary concrete (OC) has a $\sum_R$ of 0.093 cm²/g, basalt magnetite (BM) has 0.111 cm²/g, steel magnetite (SM) has 0.142 cm²/g, and ZBSS50 has 0.112 cm²/g. This comparison highlights the exceptional shielding performance of ZBSS50 against fast neutrons, surpassing other materials in the series, except for steel magnetite (SM). This superior shielding capability makes ZBSS50 an ideal material for applications where radiation protection is paramount, such as in nuclear facilities, medical radiation therapy, and other high-radiation environments.

4. Conclusion

This study investigated the mechanical, photon, and neutron attenuation properties of samarium-doped zinc bismuth silicate (ZBSS) glasses. The linear attenuation coefficient (LAC) was evaluated using Phy-X/PSD, revealing that ZBSS10, with the highest Bi_2O_3 content, exhibited the highest LAC due to enhanced photon absorption. The LAC values decreased with lower Bi_2O_3 content and with increasing photon energy, as higher-energy photons penetrate more deeply into the glass. Additionally, ZBSS10 demonstrated the lowest half-value layer (HVL), which offers advantages in reducing material cost and weight for radiation shielding applications. The radiation protection efficiency (RPE) analysis highlighted a significant correlation between the thickness of ZBSS glasses and their radiation attenuation capabilities. Notably, ZBSS10 achieved equivalent radiation reduction with a smaller thickness compared to ZBSS50; specifically, at a photon energy of 0.2506 MeV, a thickness of 0.205 cm of ZBSS10 was sufficient to attenuate photons by 25%, while ZBSS50 required an additional 22.4% increase in thickness (from 0.205 cm to 0.2507 cm) to achieve the same reduction. These findings highlight the importance of composition and thickness in optimizing radiation protection

Conflict of interest

The authors declare no conflict of interest.

Acknowledgements

The authors thank TETFund Nigeria for funding their Ph.D. program and University Technology Malaysia's for providing an enabling environment.

References

1. AbuAlRoos, N.J., N.A.B. Amin, and R. Zainon, *Conventional and new lead-free radiation shielding materials for radiation protection in nuclear medicine: A review.* Radiat. Phys. Chem., 2019. **165**: p. 108439.
2. Al-Buriahi, M.S., I. Olarinoye, S. Alomairy, I. Kebaili, R. Kaya, H. Arslan, and B.T. Tonguc, *Dense and environment friendly bismuth barium telluroborate glasses for nuclear protection applications.* Prog. Nucl. Energy, 2021. **137**: p. 103763.
3. Kaur, P., D. Singh, and T. Singh, *Heavy metal oxide glasses as gamma rays shielding material.* Nuclear Engineering and design, 2016. **307**: p. 364-376.
4. Usman, I., S.M. Sanusi Mohd, and E.N. Ahmad, *Investigation of the optical and radiation shielding parameters of erbium-doped zinc sodium tungsten borate glass using MCNP5 simulations.* Materials Research Express, 2024. https://iopscience.iop.org/article/10.1088/2053-1591/ad8b14
5. Singh, K., N. Singh, R. Kaundal, and K. Singh, *Gamma-ray shielding and structural properties of PbO–SiO2 glasses.* Nucl Instrum Methods Phys Res B NUCL INSTRUM METH B, 2008. **266**(6): p. 944-948.
6. Duée, C., F. Désanglois, I. Lebecq, and C. Follet-Houttemane, *Predicting glass transition and crystallization temperatures of silicate bioglasses using mixture designs.* J. Non·Cryst. Solids, 2012. **358**(8): p. 1083-1090.
7. Ibrahim, A., M. Farag, and M. Sadeq, *Towards highly transparent tungsten zinc sodium borate glasses for radiation shielding purposes.* Ceram. Int., 2022. **48**(9): p. 12079-12090.
8. Kharitonova, E., E. Orlova, N. Gorshkov, V. Goffman, S. Chernyak, and V. Voronkova, *Polymorphism and conductivity of Bi2O3-based fluorite-like compounds in Bi2O3–Nd2O3–MoO3 system.* J. Alloys Compd., 2019. **787**: p. 452-462.
9. Liu, S., S. Kang, H. Wang, G. Wang, H. Zhao, and W. Cai, *Nanosheets-built flowerlike micro/nanostructured Bi2O2. 33 and its highly efficient iodine removal performances.* Chemical engineering journal, 2016. **289**: p. 219-230.
10. Abou Hussein, E., A. Madbouly, and N. El Alaily, *Gamma ray interaction of optical, chemical, physical behavior of bismuth silicate glasses and their radiation shielding proficiency using Phy-X/PSD program.* J. Non·Cryst. Solids, 2021. **570**: p. 121021.
11. Elkhoshkhany, N., S. Marzouk, M. El–Sherbiny, M. Atef, K. Damak, M.S. Alqahtani, H. Algarni, and M. Reben, *Spectroscopic properties in simple cost glasses with alkaline oxides doped with Sm2O3 for display laser emission.* Results Phys., 2021. **31**: p. 104955.
12. Abouhaswa, A., M. Sayyed, A.S. Altowyan, Y. Al-Hadeethi, and K. Mahmoud, *Synthesis,*

 © 2024 Faculty of Science, Sokoto State University, Sokoto.

structural, optical and radiation shielding features of tungsten trioxides doped borate glasses using Monte Carlo simulation and phy-X program. J. Non·Cryst. Solids, 2020. **543**: p. 120134.
13. Al-Buriahi, M., Y. Alajerami, A. Abouhaswa, A. Alalawi, T. Nutaro, and B. Tonguc, *Effect of chromium oxide on the physical, optical, and radiation shielding properties of lead sodium borate glasses.* J. Non·Cryst. Solids, 2020. **544**: p. 120171.
14. Pal, I., A. Agarwal, S. Sanghi, and M. Aggarwal, *Investigation of spectroscopic properties, structure and luminescence spectra of Sm3+ doped zinc bismuth silicate glasses.* Spectrochimica Acta Part A: Molecular and Biomolecular Spectroscopy, 2013. **101**: p. 74-81.
15. Khattari, Z., N.A. Alsaif, Y. Rammah, E. Abou Hussein, M. Shams, and R. Elsad, *Fabrication, physical, mechanical, and radiation protection properties of bismo-borate glasses containing La3++ Eu3+ as additive ions.* Radiat. Phys. Chem., 2022. **201**: p. 110454.
16. Inaba, S., S. Fujino, and K. Morinaga, *Young's modulus and compositional parameters of oxide glasses.* J. Am. Ceram. Soc., 1999. **82**(12): p. 3501-3507.
17. Al-Buriahi, M., T. Taha, M.A. Alothman, H. Donya, and I. Olarinoye, *Influence of WO3 incorporation on synthesis, optical, elastic and radiation shielding properties of borosilicate glass system.* Eur. Phys. J. Plus . 2021. **136**(7): p. 779.
18. Şakar, E., Ö.F. Özpolat, B. Alım, M. Sayyed, and M. Kurudirek, *Phy-X/PSD: development of a user friendly online software for calculation of parameters relevant to radiation shielding and dosimetry.* Radiat. Phys. Chem., 2020. **166**: p. 108496.
19. Saleh, E.E., M.A. Algradee, S. El-Fiki, and G. Youssef, *Fabrication of novel lithium lead bismuth borate glasses for nuclear radiation shielding.* Radiat. Phys. Chem., 2022. **193**: p. 109939.
20. Kumar, A., D. Gaikwad, S.S. Obaid, H. Tekin, O. Agar, and M. Sayyed, *Experimental studies and Monte Carlo simulations on gamma ray shielding competence of (30+ x) PbO10WO3 10Na2O− 10MgO–(40-x) B2O3 glasses.* Prog. Nucl. Energy, 2020. **119**: p. 103047.
21. Iliyasu, U., A. Shehu, and A. Rufaâ, *Effect of MnO2 on the optical, elastic, mechanical, and radiation shielding performance of bismuth silicate glass.* Caliphate Journal of Science and Technology, 2024. **6**(2): p. 121-130. https://doi.org/10.4314/cajost.v6i2.1
22. Agar, O., M. Sayyed, F. Akman, H. Tekin, and M. Kaçal, *An extensive investigation on gamma ray shielding features of Pd/Ag-based alloys.* Nucl. Eng. Technol., 2019. **51**(3): p. 853-859.
23. Iliyasu, U. and A. Shehu, *Photon and Neutron Characterization of Titanium Neodymium Tellurite Glass Doped WO3.* Caliphate Journal of Science and Technology, 2024. **6**(2): p. 236-248. https://doi.org/10.4314/cajost.v6i2.13
24. Yasmin, S., M. Khandaker, D. Bradley, H. Osman, A. Alyahyawi, M. Sayyed, M. Faruque, K. Naseer, and A.M. Idris, *The efficacy of various thicknesses of float glasses for protection of gamma-radiation.* Radiat. Phys. Chem., 2022. **199**: p. 110301.
25. Nagai, R., T. Honma, and T. Komatsu, *Laser patterning of ZnO crystals on the surface of borosilicate glass.* J. Am. Ceram. Soc., 2010. **93**(3): p. 658-661.
26. Almuqrin, A.H., M. Sayyed, N.S. Prabhu, and S.D. Kamath, *Influence of Bi2O3 on mechanical properties and radiation-shielding performance of lithium zinc bismuth silicate glass system using Phys-X software.* Materials, 2022. **15**(4): p. 1327.
27. El Abd, A., G. Mesbah, N.M. Mohammed, and A. Ellithi, *A simple method for determining the effective removal cross section for fast neutrons.* J. Radiat. Nucl. Appl, 2017. **2**(2): p. 53-58.

 © 2024 Faculty of Science, Sokoto State University, Sokoto.